









Is [Y/Mg] a Reliable Age Diagnostic for FGK Stars?

Travis A. Berger^{1,2,4} , Jennifer L. van Saders² , Daniel Huber² , Eric Gaidos³ , Joshua E. Schlieder¹ , and Zachary R. Claytor² 

¹Exoplanets and Stellar Astrophysics Laboratory, Code 667, NASA Goddard Space Flight Center, Greenbelt, MD 20771, USA; travis.a.berger@nasa.gov

²Institute for Astronomy, University of Hawai'i, 2680 Woodlawn Drive, Honolulu, HI 96822, USA

³Department of Earth Sciences, University of Hawai'i at Mānoa, Honolulu, HI 96822, USA

Received 2022 June 3; revised 2022 August 3; accepted 2022 August 3; published 2022 September 6

Abstract

Current spectroscopic surveys are producing large catalogs of chemical abundances for stars of all types. The yttrium-to-magnesium ratio, [Y/Mg], has emerged as a candidate age indicator for solar twins in the local stellar neighborhood. However, it is unclear whether it is a viable age diagnostic for more diverse stellar types, so we investigate [Y/Mg] as an age indicator for the FGK-type planet host stars observed by Kepler. We find that the [Y/Mg] “Clock” is most precise for solar twins, with a [Y/Mg]/age slope of $m = -0.0370 \pm 0.0071$ dex Gyr⁻¹ and $\sigma_{\text{Age}} = 2.6$ Gyr. We attribute the lower precision compared to literature results to nonsolar twins contaminating our solar twin sample and recommend a 1.5 Gyr systematic uncertainty for stellar ages derived with any [Y/Mg]–Age relation. We also analyzed the [Y/Mg] Clock as a function of T_{eff} , $\log g$, and metallicity individually and find no strong trends, but we compute statistically significant [Y/Mg]–Age relations for subsamples defined by ranges in T_{eff} , $\log g$, and metallicity. Finally, we compare [Y/Mg] and rotation ages and find statistically similar trends as for isochrone ages, although we find that rotation ages perform better for GK dwarfs while isochrones perform better for FG subgiants. We conclude that the [Y/Mg] Clock is most precise for solar twins and analogs but is also a useful age diagnostic for FGK stars.

Unified Astronomy Thesaurus concepts: [Stellar evolutionary models \(2046\)](#); [Chemical abundances \(224\)](#); [Abundance ratios \(11\)](#); [Stellar properties \(1624\)](#); [Stellar ages \(1581\)](#); [Stellar rotation \(1629\)](#); [Planet hosting stars \(1242\)](#)

1. Introduction

Stellar ages are invaluable for interpreting the sequence of events in the universe. However, stellar ages are typically very difficult to estimate for field stars (Soderblom 2010). Field-star ages have been determined through isochrone comparison (or placement in a color–magnitude diagram; Edvardsson et al. 1993; Nordström et al. 2004; Holmberg et al. 2009; Morton et al. 2016; Johnson et al. 2017), now more powerful with Gaia parallaxes (Fulton & Petigura 2018; Berger et al. 2018b, 2020b, 2020a), to gyrochronology (Barnes 2007; Mamajek & Hillenbrand 2008; van Saders et al. 2016; Angus et al. 2018; Curtis et al. 2019), to asteroseismology (Mazumdar 2005; Oti Floranes et al. 2005; Kjeldsen et al. 2008; Silva Aguirre et al. 2015; Creevey et al. 2017; Pinsonneault et al. 2018), and to galactic kinematics (Makarov 2007; Fernández et al. 2008; Angus et al. 2020; Lu et al. 2021).

Stellar ages can also be inferred from chemical abundances, such as lithium abundances (Skumanich 1972; Soderblom et al. 1993; Sestito & Randich 2005; Mentuch et al. 2008; Boesgaard et al. 2016; Berger et al. 2018a; Deepak 2019; Gaidos et al. 2020; Magrini et al. 2021), which are expected to evolve either during the lifetime of a star or over the lifetimes of many stars as they enrich the interstellar medium from which new stars are born. By measuring elemental abundance ratios in stellar atmospheres, we can infer the composition of the cloud of dust and gas from which

the stars were born and the nucleosynthetic pathways that could have produced such compositions (Johnson 2019). These data, compared to galactic chemical evolution (GCE) models based on empirical calibrations, enable us to infer stellar ages.

[Y/Mg], the yttrium (Y) to magnesium (Mg) abundance ratio of a star relative to the Sun, has been proposed as an age diagnostic for solar-type stars (da Silva et al. 2012; Nissen 2015; Tucci Maia et al. 2016). As an α -element, Mg is produced primarily by the core-collapse supernovae of massive stars ($M_{\star} > 8 M_{\odot}$) with minor contributions from intermediate-mass stars ($2 M_{\odot} < M_{\star} < 8 M_{\odot}$; Vangioni & Olive 2019). Massive stars burn through their hydrogen much more quickly than their low-mass counterparts and hence are expected to have populated the interstellar medium with larger abundances of α -elements at earlier times. In contrast, intermediate-mass stars produce elements such as Y through the slow neutron capture process (s -process) during their asymptotic giant branch phase. This is shortly before they expel their envelopes into the surrounding interstellar medium. Because intermediate-mass stars have longer evolutionary timescales owing to their lower hydrogen-burning rates, enrichment of s -process elements in the interstellar medium and eventual stellar atmospheres is expected to occur at later times in our Galaxy’s evolution relative to the α -elements. Therefore, the principles of GCE predict that [Y/Mg] has increased with time such that it decreases with stellar age.

According to Nissen (2015), Tucci Maia et al. (2016, hereafter TM16), and Spina et al. (2016), [Y/Mg] is a precise clock for solar twins, defined as stars within ± 100 K of solar T_{eff} and within ± 0.1 dex in $\log g$ and metallicity [Fe/H] (Ramírez et al. 2014). TM16 shows that differential measurements of [Y/Mg] can produce ages as precise as 0.8 Gyr for solar twins. More recent work has corroborated the [Y/Mg]

⁴ NASA Postdoctoral Program Fellow.

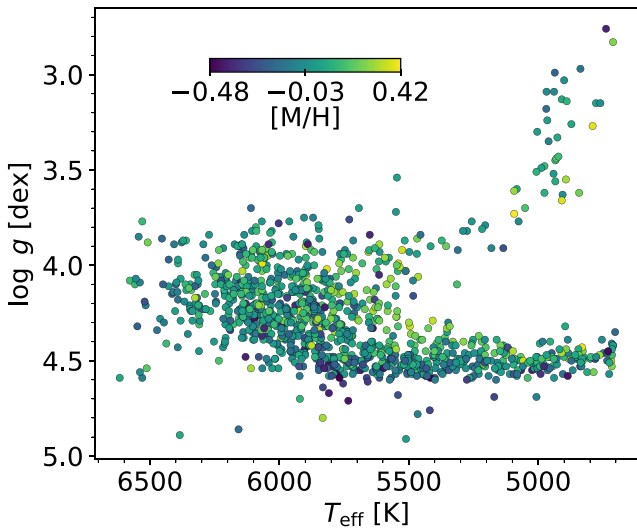


Figure 1. Kiel diagram of 1100 Kepler planet host stars with self-consistent spectroscopic T_{eff} , $\log g$, $[M/H]$, $[Y/Mg]$, and age measurements from Brewer & Fischer (2018). Stars are colored according to spectroscopic $[M/H]$ as determined by Brewer & Fischer (2018).

“Clock” for solar-type stars (Anders et al. 2018) and those with T_{eff} between 5700 and 6400 K (Nissen et al. 2017), evolved solar-metallicity stars (Slumstrup et al. 2017; Casamiquela et al. 2021), thin- and thick-disk stars (Titarenko et al. 2019), and stars in the solar- and outer-disk regions of the Galaxy (Viscasillas Vázquez et al. 2022). However, Feltzing et al. (2017) find that the $[Y/Mg]$ Clock may only be useful within a narrow range of $[Fe/H]$ and show that the relation is effectively flat for metallicities of ≈ -0.5 dex, and Viscasillas Vázquez et al. (2022) show that the Clock changes as a function of galactocentric distance. Similarly, while Titarenko et al. (2019) also find a tight correlation between $[Y/Mg]$ and age, a difference in slopes for thin- and thick-disk stars suggests that the $[Y/Mg]$ Clock is not universal and is instead Galactic neighborhood dependent. Therefore, it is unclear how useful the $[Y/Mg]$ Clock is for the wider range of T_{eff} , $\log g$, and $[Fe/H]$ present in field stars. Here we use the well-studied Kepler (Borucki et al. 2010) planet host stars with high-resolution spectra and rotation periods to test this relation.

2. Stellar Sample

In Figure 1, we plot the Kepler host star sample with measured T_{eff} , $\log g$, metallicity, yttrium abundance ($A(Y)$), and magnesium abundance ($A(Mg)$) from Brewer & Fischer (2018). Brewer & Fischer (2018) used Spectroscopy Made Easy (SME; Piskunov & Valenti 2017) to derive the stellar atmospheric parameters and abundances. We removed three stars with metallicities below -0.5 dex (poor statistics). The remaining 1100 FGK stars have metallicities ranging from -0.48 to 0.42 dex, and most are dwarfs, although a few have started evolving up the giant branch. Unlike the solar twin samples from Nissen (2015), TM16, and Spina et al. (2016), this plot includes both more evolved stars and stars of spectral types F and K.

In addition to $[Y/Mg]$ measurements, we also adopt the stellar ages from Brewer & Fischer (2018, hereafter BF18), which are self-consistent with the derived spectroscopic parameters and elemental abundances. BF18 used isochrones (Morton 2015) to infer fundamental stellar parameters including age from a combination of the spectroscopic parameters detailed above,

Gaia DR2 parallaxes (Gaia Collaboration et al. 2018), Two Micron All Sky Survey K_s magnitudes (Skrutskie et al. 2006), and Dartmouth Stellar Evolution Database models (Dotter et al. 2008). Fulton & Petigura (2018) also inferred fundamental parameters for the same stellar sample, but they did not measure $[Y/Mg]$, the central abundance ratio of this work. Therefore, we choose to use the inherently self-consistent atmospheric parameters, abundances, and stellar ages of BF18 to minimize potential systematics between data sets. We will also compare the asteroseismic ages determined for the 34 Kepler planet host stars in common with BF18 from Silva Aguirre et al. (2015) and Creevey et al. (2017).

3. $[Y/Mg]$ and Age as a Function of Spectroscopic Parameters

An important first step is to test whether $[Y/Mg]$ correlates with spectroscopic parameters independently of age. Figure 2 shows age as a function of T_{eff} , $\log g$, and metallicity. As expected, ages increase for cool stars with lower surface gravities and more metal-poor stars. Additionally, the age scatter is largest for cool main-sequence stars. This behavior is expected owing to the strong relationship between stellar mass and stellar lifetimes.

The bottom panels of Figure 2 show $[Y/Mg]$ versus the spectroscopic parameters. Compared to the trends seen in the age plots, the $[Y/Mg]$ trends shown here are weaker yet still significant. In particular, we see the smallest $[Y/Mg]$ abundances at low T_{eff} and the largest $[Y/Mg]$ abundances at high T_{eff} , although around solar T_{eff} the median bins do not vary much. Most of the differences in median-binned T_{eff} occur for the coolest and hottest stars, although they do have larger uncertainties given their smaller relative number. We see $[Y/Mg]$ increase for $\log g$ below 4.0 dex and peak at $[M/H] \approx 0.0$ dex, with gradual and/or insignificant trends otherwise. In addition, we note that some natural systematic correlations are expected if $[Y/Mg]$ is related to age, given how age is correlated with T_{eff} and $\log g$ through the stellar lifetime and how overall metallicity should differ as a function of $[Y/Mg]$, given their similar observables. Ultimately, the systematics shown here are important to consider when interpreting trends of $[Y/Mg]$ as a function of stellar age.

4. $[Y/Mg]$ as a Function of Stellar Age

Figure 3 compares $[Y/Mg]$ versus age for the TM16, BF18, and asteroseismic host star samples. While all data sets show $[Y/Mg]$ decreasing with age, the Kepler host star BF18 and asteroseismic correlation coefficients are weaker ($R^2 = 0.27$ and 0.23 , respectively, vs. 0.89 for TM16) with larger scatter ($\sigma = 0.14$ and 0.12 dex, respectively, vs. 0.04 dex for TM16). At least some of the additional scatter can be explained by the difference in typical $[Y/Mg]$ uncertainties (0.02 dex for TM16 vs. 0.05 dex for BF18). This difference occurs because TM16 performed differential abundance analyses with respect to the Sun, an approach only valid for solar twins, whereas BF18 did not. Still, the 0.1 dex difference in scatter is not covered by the 0.03 dex difference in typical $[Y/Mg]$ uncertainties, which means that there must be either astrophysical scatter introduced by the diverse FGK hosts in BF18 or additional systematics. The formal uncertainties on the isochrone ages reported by both BF18 and TM16 appear to be similar to those of the asteroseismic ages, which is likely due to the small T_{eff}

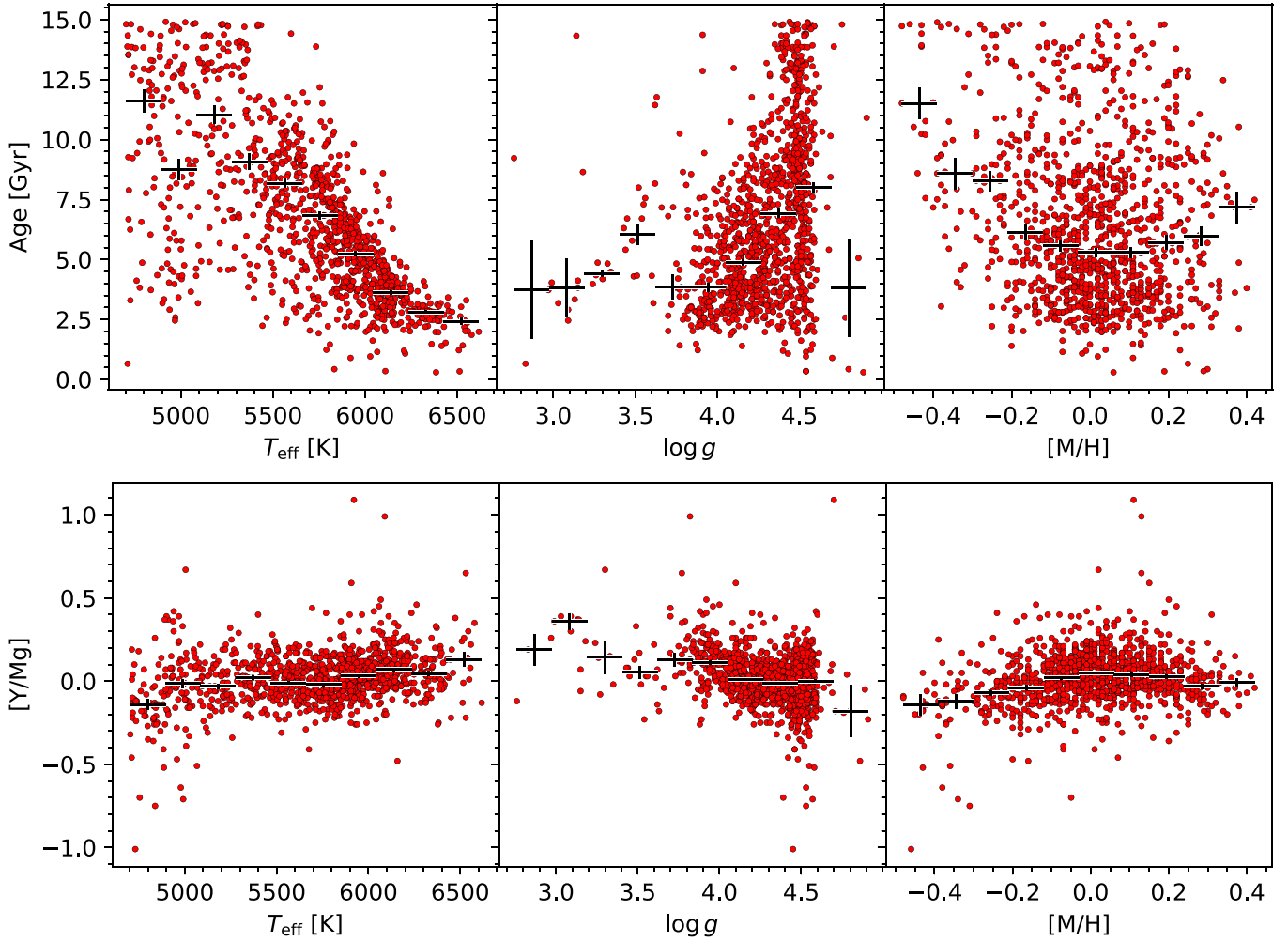


Figure 2. Top: age as a function of T_{eff} , $\log g$, and metallicity for the BF18 sample. Median ages for each bin are shown as plus signs, and vertical bars represent the standard error of the mean for each bin. Bottom: [Y/Mg] as a function of the spectroscopic parameters for the BF18 sample. We omitted stars with metallicities < -0.5 because of their sparseness.

uncertainties used in both isochrone analyses. Systematics in the reported ages are likely much larger (Tayar et al. 2022). In addition, the BF18 hosts display a larger scatter in [Y/Mg] at the oldest ages.

TM16 report the following best-fit linear relation:

$$[\text{Y}/\text{Mg}] = 0.184(\pm 0.008) - 0.041(\pm 0.001) \times \text{Age}, \quad (1)$$

where the age is in Gyr. Given the uncertainties on the best-fit slope and intercept, this implies a tight correlation between age and [Y/Mg]. To test the robustness of this result, we performed linear fits while accounting for x - and y -uncertainties using emcee (Foreman-Mackey et al. 2013) and implemented the following likelihood function (Hogg et al. 2010):

$$\ln \mathcal{L} = -\frac{1}{2} \sum_{i=1}^N \ln(\Sigma_i^2 + V) - \frac{1}{2} \sum_{i=1}^N \frac{\Delta_i^2}{\Sigma_i^2 + V}, \quad (2)$$

where

$$\begin{aligned} \Delta_i &= \hat{v}^\top Z_i - b \cos \theta, \\ \Sigma_i &= \hat{v}^\top S_i \hat{v}, \\ V &= c^2 \cos^2 \theta, \end{aligned} \quad (3)$$

and where

$$\hat{v} = \begin{bmatrix} -\sin \theta \\ \cos \theta \end{bmatrix}, \quad Z_i = \begin{bmatrix} x_i \\ y_i \end{bmatrix}, \quad S_i = \begin{bmatrix} \sigma_{x_i}^2 & \sigma_{x_i} \sigma_{y_i} \\ \sigma_{x_i} \sigma_{y_i} & \sigma_{y_i}^2 \end{bmatrix}, \quad (4)$$

with the slope m parameterized as $\theta = \arctan(m)$ and the best-fit model parameterized as $b \cos \theta$ to treat all possible slopes equally. Δ represents the residuals, and Σ is the covariance rotated parallel to the slope. c is a measure of the point-to-point scatter not contained within the formal uncertainties in units of dex, and we may refer to it as the intrinsic scatter from now on.

We used 32 walkers with 20,000-step chains in the three-dimensional parameter space with uniform priors on the slope ($-1 \text{ dex Gyr}^{-1} < m < 1 \text{ dex Gyr}^{-1}$), intercept ($-2 \text{ dex} < b < 2 \text{ dex}$), and additional [Y/Mg] scatter ($-20 < \ln c < 5$) as our free parameters. We used emcee's `get_autocorr_time()` function to ensure that the fits converged within the first 400 steps of sampling. We then identified the longest autocorrelation time of our three free parameters and removed four times that number of steps to account for burn-in. Examples of the best-fit relations for each data set are shown in Figure 3. We also ran 1000 bootstrap simulations to quantify the impact of outliers on the fit parameters. In particular, we ran each bootstrap simulation by drawing, with replacement, the same number of stars as the observed sample and

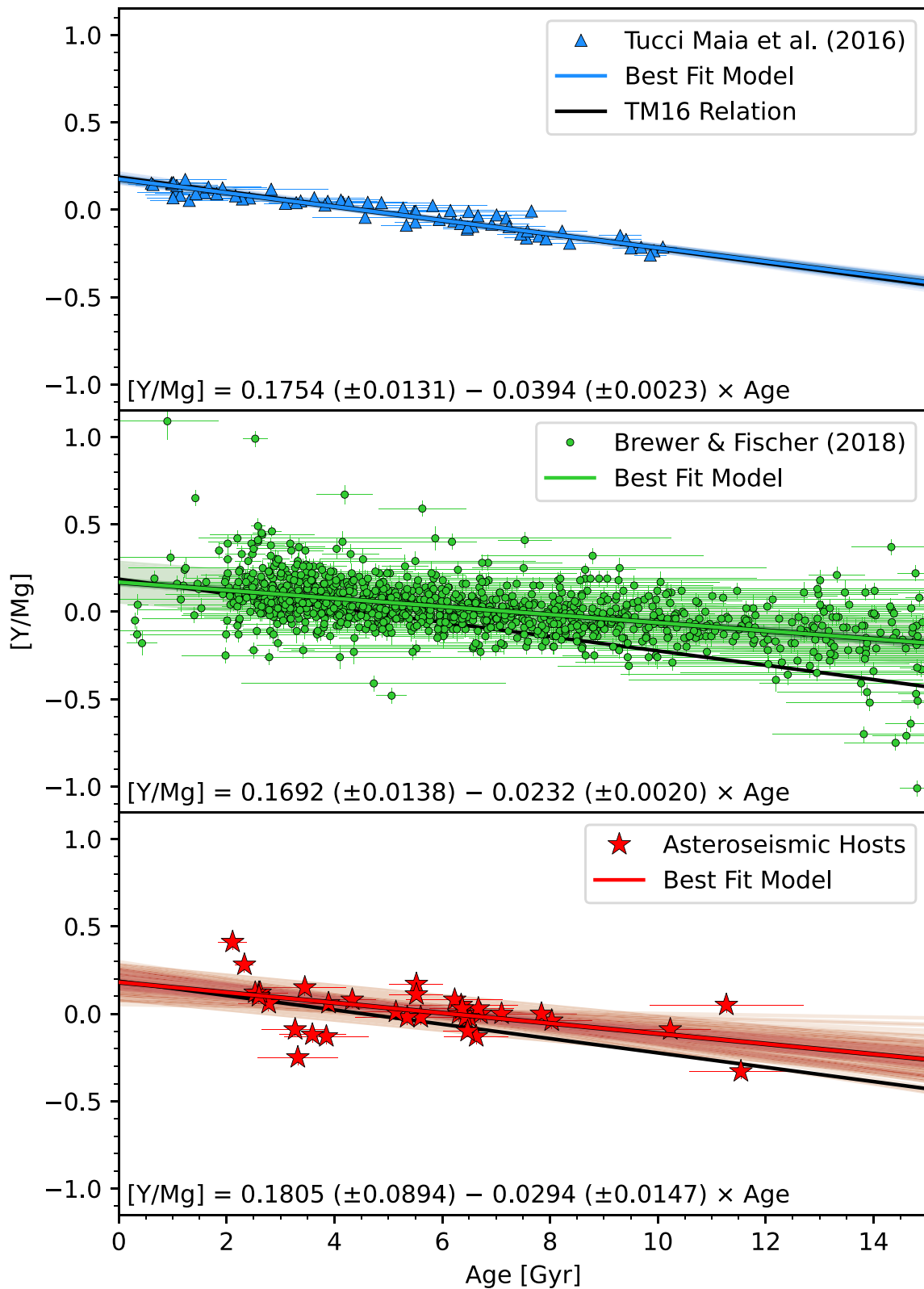


Figure 3. $[Y/Mg]$ vs. stellar age for three samples: (1) **TM16** solar twins with solar-differential $[Y/Mg]$ abundances from the Ramírez et al. (2014) analysis of MIKE spectra (Bernstein et al. 2003) and Yonsei-Yale isochrone ages (Yi et al. 2001; top), (2) **BF18** Kepler planet host stars with $[Y/Mg]$ abundances and isochrone ages based on Dartmouth Stellar Evolution Database (DSEP; Dotter et al. 2008; middle), and (3) Kepler planet host stars with asteroseismic ages from Silva Aguirre et al. (2015) or Creevey et al. (2017) and Brewer & Fischer 2018 $[Y/Mg]$ abundances (bottom). Individual MCMC realizations are shown as the color-matched translucent curves, and the intrinsic scatters are shown as the lightly shaded regions surrounding the best-fit model (where visible). In black is the best-fit expression from **TM16**, and uncertainties are plotted for each individual star.

Table 1
[Y/Mg]–Isochrone Age Best-fit Relations

Sample	Slope (m)	σ_m	Intercept (b)	σ_b	Intrinsic Scatter (c)	σ_{age} (Gyr)	F -test (σ)
1. TM16	−0.0394	0.0023	0.175	0.013	<0.001	0.95	12.4
2. BF18	−0.0232	0.0020	0.169	0.014	0.12	5.8	18.6
3. Asteroseismic	−0.029	0.015	0.181	0.089	0.10	6.1	2.9
4. BF18 solar analogs	−0.0359	0.0055	0.219	0.036	0.001	2.6	6.1
5. BF18 solar twins	−0.0370	0.0071	0.231	0.043	<0.001	2.6	4.2
6. Reliable BF18 sample ($T_{\text{eff}} > 5400$ K)	−0.0245	0.0025	0.171	0.015	0.10	5.0	14.5
7. Reliable BF18 sample $\cap T_{\text{eff}} > 5872$ K	−0.0366	0.0062	0.216	0.029	0.12	3.8	8.9
8. Reliable BF18 sample $\cap 5672$ K $\leq T_{\text{eff}} \leq 5872$ K	−0.0307	0.0050	0.197	0.035	0.071	3.5	8.6
9. Reliable BF18 sample $\cap T_{\text{eff}} < 5672$ K	−0.0224	0.0037	0.182	0.031	0.063	4.5	7.4
10. Reliable BF18 sample $\cap \log g < 4.34$	−0.0309	0.0037	0.205	0.021	0.11	3.9	11.8
11. Reliable BF18 sample $\cap 4.34 \leq \log g \leq 4.54$	−0.0201	0.0033	0.137	0.022	0.078	5.3	7.9
12. Reliable BF18 sample $\cap \log g > 4.54$	−0.0180	0.0090	0.131	0.078	0.17	14	3.0
13. Reliable BF18 sample $\cap [M/H] > 0.2$	−0.0190	0.0059	0.130	0.040	0.080	5.9	5.2
14. Reliable BF18 sample $\cap -0.2 \leq [M/H] \leq 0.2$	−0.0246	0.0033	0.177	0.019	0.11	5.2	11.4
15. Reliable BF18 sample $\cap [M/H] < -0.2$	−0.0163	0.0054	0.068	0.046	0.096	8.0	3.5

Note. Best-fit relations computed for the various [Y/Mg]–isochrone age comparisons detailed in this paper. All equations are of the form $[Y/Mg] = m \times \text{age} + b$, and 1σ uncertainties are quoted for each parameter. We fit for intrinsic scatter by adding the term $c^2 \cos^2(\arctan(m))$ to the variance in our MCMC analysis (see Section 4) and report σ_{age} , which is the corresponding scatter in age in units of Gyr about the best-fit relation. We also include our F -test results in the final column, indicating the corresponding significance of the p -value in units of σ at which the data prefer two-parameter fits (slope plus intercept) over one-parameter fits (intercept only). We plot the summary statistics for this table’s rows 1–15 in columns 1–15 of Figure 13, respectively.

then used `scipy`’s `minimize` function to determine the maximum likelihood fit parameters from the likelihood in Equation (2). We then computed the standard deviation of the 1000 bootstrapped slopes and intercepts and then added them in quadrature to the MCMC uncertainties to produce our reported uncertainties:

$$\begin{aligned}\sigma_m &= \sqrt{\sigma_{m,\text{MCMC}}^2 + \sigma_{m,\text{BOOT}}^2}, \\ \sigma_b &= \sqrt{\sigma_{b,\text{MCMC}}^2 + \sigma_{b,\text{BOOT}}^2},\end{aligned}\quad (5)$$

where σ_{MCMC}^2 and σ_{BOOT}^2 represent uncertainties derived from the MCMC and bootstrap analyses, respectively.

The top panel in Figure 3 shows our best-fit relation for the **TM16** sample. We compute a slope of $m = -0.0394 \pm 0.0023$ dex Gyr $^{-1}$ and an intercept of $b = 0.175 \pm 0.013$ dex, which matches Equation (1) within uncertainties. This result is in statistical agreement with the reported relation of **TM16**, and the slope is still significant at $\approx 17\sigma$, despite the differences in our methods.

The middle panel of Figure 3 displays the Kepler planet host star sample with stellar ages from **BF18**. Our best-fit relation for the 1100-star sample has a slope $m = -0.0232 \pm 0.0020$ dex Gyr $^{-1}$, significant at $\approx 12\sigma$, which is shallower and has significantly more intrinsic scatter ($c = 0.12$ dex) than the **TM16** relation. The shallow slope computed here suggests that the [Y/Mg] Clock may not be as strong an age diagnostic as previously reported, at least for the wide range of T_{eff} , $\log g$, and metallicities present in the **BF18** Kepler host star sample. In addition, the large c here indicates that there is true astrophysical and/or systematic scatter introduced by the diverse FGK star sample.

The bottom panel of Figure 3 shows the best-fit relation for the asteroseismic stars from Silva Aguirre et al. (2015) and Creevey et al. (2017). The slope, at $m = -0.029 \pm 0.015$ dex Gyr $^{-1}$, is consistent with the **BF18** and **TM16** relations, as the smaller sample size and large intrinsic scatter ($c = 0.10$ dex) produce a more uncertain [Y/Mg] Clock when compared to the significantly

larger **BF18** and tighter **TM16** samples. We compile our best-fit [Y/Mg]–age relations and uncertainties in Table 1.

To determine each relation’s subsequent uncertainty in stellar age, we performed similar MCMC analyses where we define age as the ordinate and [Y/Mg] as the abscissa, with uniform priors on the slope (-100 Gyr dex $^{-1} < m < 10$ Gyr dex $^{-1}$), intercept (-10 Gyr $< b < 100$ Gyr), and intrinsic scatter ($-20 < \ln c < 3$). The subsequent best-fit relations produce residuals with scatters of 0.95, 5.8, and 6.1 Gyr in age for the **TM16**, **BF18**, and asteroseismic samples, respectively.

We also performed F -tests using `scipy`’s `stats.f` to determine the significance at which a two-parameter (slope + intercept) model is better than a one-parameter (intercept-only) model. The intercept-only model assumes a flat slope and hence no [Y/Mg]–age dependence. For the **TM16**, **BF18**, and asteroseismic data, we compute p -values consistent with 12.4σ , 18.6σ , and 2.9σ significances, respectively. Therefore, the **TM16** and **BF18** data statistically prefer the slope + intercept model at $\gg 3\sigma$ significance over the intercept-only model, while the asteroseismic data prefer the slope + intercept model with marginal significance due to their small sample size and large scatter. While we acknowledge the large discrepancy between the 12σ F -test and the 17σ slope for the **TM16** data, we note that the magnitude of [Y/Mg] uncertainties significantly affects the precision of the MCMC-derived parameters, while it has little to no impact on the F -test results.

4.1. The [Y/Mg] Clock for Kepler Solar Twins and Analogs

We now isolate a subsample of **BF18** stars that is consistent with solar twins and analogs. We use the same definition of solar twin as **TM16** and Ramírez et al. (2014): ± 100 K in T_{eff} and ± 0.1 dex in $\log g$ and [M/H]. Because our sample’s uncertainties are larger than those of **TM16**, our solar twins and analogs will be more contaminated by nontwin stars, which may produce flatter [Y/Mg]–age relations. We found no solar twins with asteroseismic constraints in our overlapping sample.

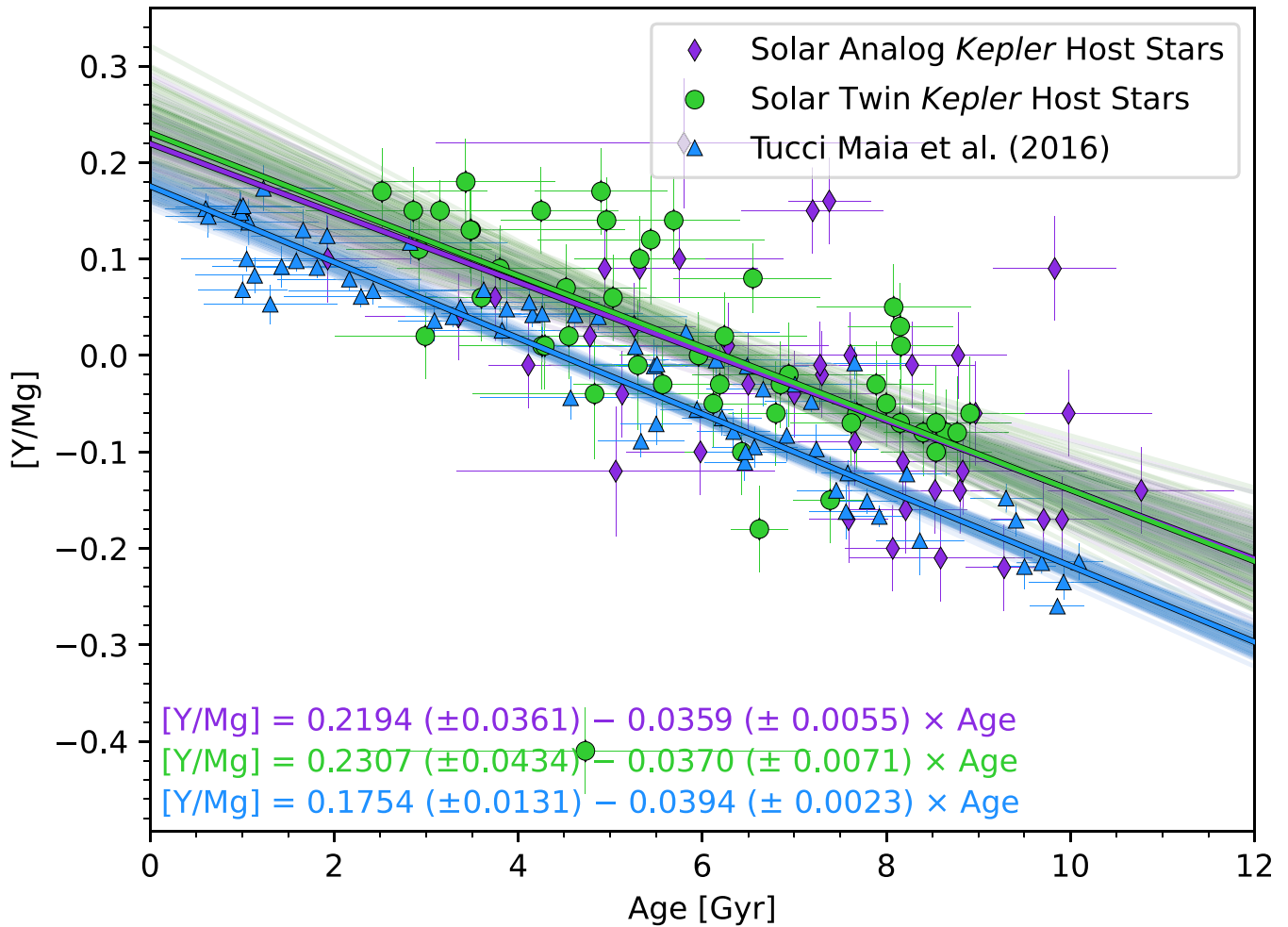


Figure 4. $[Y/Mg]$ vs. age for Kepler solar twins (green circles), defined as stars within ± 100 K in T_{eff} and ± 0.1 dex in $\log g$ and $[M/H]$ relative to the Sun. Solar analogs (purple diamonds) have similar T_{eff} and $\log g$ as the Sun, but $[M/H]$ is allowed to vary. Color-matched translucent lines show random MCMC samples. Solar twins are a subset of the solar analogs by definition and hence are plotted on top. The **TM16** relation and corresponding data are plotted in blue.

Figure 4 shows that the **BF18** solar twins, compared to **TM16**, produce a statistically similar slope (-0.0370 ± 0.0071 dex Gyr^{-1} vs. -0.0394 ± 0.0023 dex Gyr^{-1}), a $\gtrsim 1\sigma$ larger intercept (0.231 ± 0.043 dex vs. 0.175 ± 0.013 dex), and similar intrinsic scatters (both less than 0.001 dex). Unsurprisingly, the **BF18** solar twin $[Y/Mg]$ -age relation is more similar to **TM16** compared to the full **BF18** sample in Figure 3. When using different $[Y/Mg]$ -age relations, a significant intercept offset for relations with equivalent slopes will also produce significantly different ages. We compute a 2.6 Gyr uncertainty in age from the **BF18** solar twin relation, which is larger than the 0.95 Gyr uncertainty in the **TM16** relation. We note that differences in slopes, intercepts, and age uncertainties may arise from any combination of factors: (1) the **BF18** data both are more uncertain and may contain nonsolar twin contaminants, (2) **TM16** used a differential abundance analysis while **BF18** did not, and/or (3) **TM16** and **BF18** used different models to determine stellar age, which can easily produce age offsets (Tayar et al. 2022). Because we allow for intrinsic scatter, the outlier at age ≈ 5 Gyr and $[Y/Mg] \approx -0.4$ dex does not affect our best-fit line significantly.

The purple line in Figure 4 shows our best-fit relation to the **BF18** solar analogs, defined as stars within ± 100 K in T_{eff} and ± 0.1 dex in $\log g$ relative to the Sun but with varying metallicities. We compute a slope that is statistically indistinguishable from

the **TM16** relation as we did for solar twins, but the solar analogs exhibit a larger intrinsic scatter (0.001 dex) than both the **BF18** solar twins and **TM16** data. The $[Y/Mg]$ -age scatter corresponds to an uncertainty in age of 2.6 Gyr, similar to the **BF18** solar twin age uncertainty. Our measured intercept is $\gtrsim 1\sigma$ larger than the **TM16** intercept as was found for the solar twin sample above. We also note that choosing solar analogs with super- or subsolar metallicities results in a shallower $[Y/Mg]$ -age slope.

To estimate typical systematic age uncertainties given $[Y/Mg]$ for solar twins, we added our best-fit $[Y/Mg]$ -age results to those of the literature (Nissen 2015, 2016; Spina et al. 2016; Tucci Maia et al. 2016; Nissen et al. 2017) compiled in Table 6 of Delgado Mena et al. (2019). We computed a mean slope of -0.0389 ± 0.0025 dex Gyr^{-1} and a mean intercept of 0.185 ± 0.025 dex, where the uncertainties are based on the standard deviation of the various estimates. From these estimates, we then propagated our uncertainties on the slope, intercept, and $[Y/Mg]$ measurements (0.05 dex from **BF18**) to produce a 1.5 Gyr systematic uncertainty.

We conducted F -tests to compare one- and two-parameter models as before. For the **TM16** solar twins, **BF18** solar twins, and **BF18** solar analogs, we compute p -values consistent with 12.4σ , 4.2σ , and 6.1σ , respectively. Therefore, all three data sets statistically prefer the slope + intercept model at $>4\sigma$ significance.

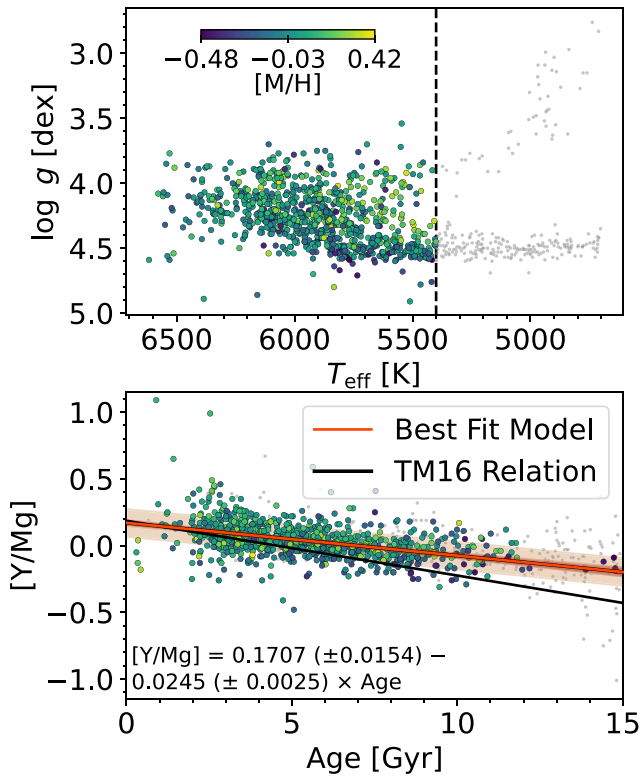


Figure 5. Top: Kiel diagram of 1100 Kepler planet host stars with self-consistent spectroscopic T_{eff} , $\log g$, $[M/H]$, $[Y/Mg]$, and age measurements from BF18. A total of 846 stars with informative ages ($T_{\text{eff}} > 5400$ K) are colored according to their spectroscopic $[M/H]$ determined by BF18, while all other stars are represented by small gray circles. Bottom: $[Y/Mg]$ versus stellar age, where stars are colored equivalently as in the top panel; the MCMC best fit is plotted in orange-red for the 846 stars with reliable ages.

4.2. A More Reliable $[Y/Mg]$ Clock Sample

Some of the increased scatter of the BF18 sample could be due to uncertainties in stellar ages. We therefore removed both lower main-sequence stars and giant stars by cutting all stars with $T_{\text{eff}} \leq 5400$ K. The lower main-sequence stars have the most uncertain isochrone ages owing to their slow evolution on the main sequence (Berger et al. 2020b, 2020a), while the systematics in giant-star ages are likely larger owing to their strong dependence on model input physics (Tayar et al. 2022).

The 846-star sample is shown in Figure 5. Our MCMC analysis produces $m = -0.0245 \pm 0.0025$ dex Gyr^{-1} , $b = 0.171 \pm 0.015$ dex, and an intrinsic scatter $c = 0.10$ dex. The slope is statistically consistent with the full sample’s slope of $m = -0.0232 \pm 0.0020$ dex Gyr^{-1} and $\approx 4\sigma$ more shallow than the TM16 slope. In addition, we determined an uncertainty of 5.0 Gyr in age compared to the full sample’s uncertainty of 5.8 Gyr. We computed an F -test p -value significance of 14.5σ , which indicates that a slope + intercept model is strongly preferred over the intercept-only model. We do not see large slope/intercept/ c differences in the reduced sample compared to the full sample above because we retain the majority of stars from the full sample, and the stars that are removed, while concentrated at old stellar ages with large variations in $[Y/Mg]$, occur roughly as frequently above and below the previous best-fit trend line. We suspect that these large $[Y/Mg]$ variations at old age arise either from difficulty in measuring $[Y/Mg]$ and/or because the majority of the removed stars are low-mass

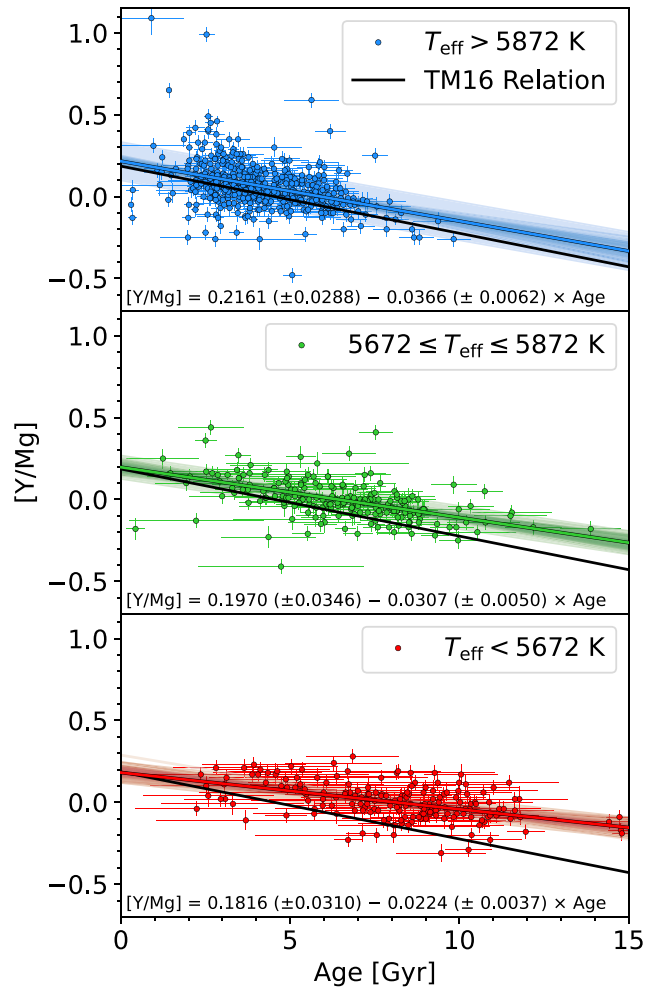


Figure 6. $[Y/Mg]$ vs. stellar age for the reduced BF18 sample. The top, middle, and bottom panels show $T_{\text{eff}} > 5872$ K, T_{eff} between 5672 and 5872 K, and $T_{\text{eff}} < 5672$ K, respectively. We plot the best-fitting relations as solid lines and the MCMC realizations as translucent lines underneath. In black we plot the TM16 best-fit relation.

dwarfs with uninformative isochrone ages due to their slow evolution in the H-R diagram.

4.3. The $[Y/Mg]$ Clock and Stellar T_{eff}

Figure 6 shows the $[Y/Mg]$ Clock for the BF18 sample split into three T_{eff} bins: (1) hotter, (2) solar, and (3) cooler stars. We observe that solar T_{eff} stars exhibit the least scatter and the most statistically significant slope with a corresponding age uncertainty of 3.5 Gyr, while the cooler stars have similar scatter with the shallowest slope and a corresponding age uncertainty of 4.5 Gyr. Comparatively, hotter stars exhibit the most scatter and produce the steepest slope with a corresponding age uncertainty of 3.8 Gyr. F -test results suggest that all three samples strongly prefer the slope + intercept model over the intercept-only fit. Table 1 lists the best-fit parameters and uncertainties.

We do not observe any strong trends in the $[Y/Mg]$ Clock as a function of T_{eff} , and we find slopes and intercepts in the hotter, solar, and cooler T_{eff} samples that are statistically consistent with one another, except for the $>1\sigma$ shallower slope for cooler T_{eff} stars relative to solar T_{eff} stars.

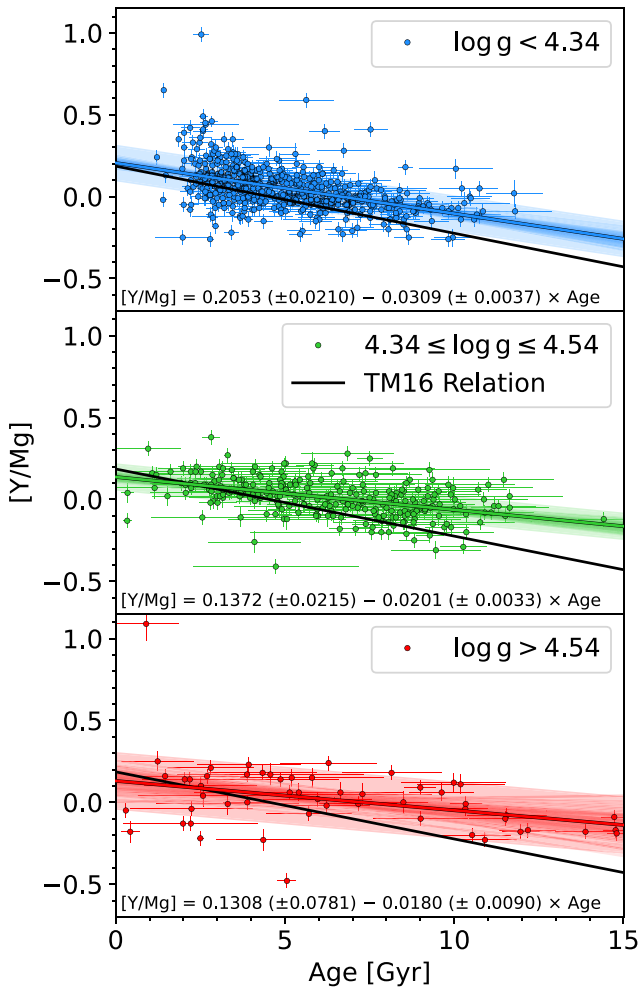


Figure 7. $[Y/Mg]$ vs. stellar age for the reduced **BF18** sample. The top, middle, and bottom panels show $\log g < 4.34$ dex, $\log g$ between 4.34 and 4.54 dex, and $\log g > 4.54$ dex, respectively. We plot the best-fitting relations as solid lines and the MCMC realizations as translucent lines underneath. In black we plot the **TM16** best-fit relation.

4.4. The $[Y/Mg]$ Clock and Stellar Surface Gravity

Similar to T_{eff} , $\log g$ provides another dimension in which to test the scope of the $[Y/Mg]$ Clock. For instance, Slumstrup et al. (2017) used open cluster data to show that the $[Y/Mg]$ –age relation derived for solar twins in Nissen (2015) holds for solar-metallicity giant stars in the core helium burning phase. Therefore, we test the relation for the Kepler dwarf and subgiant stars studied here.

Figure 7 shows the $[Y/Mg]$ Clock for stars of lower, solar, and higher $\log g$. The lower $\log g$ stars produce the statistically steepest $[Y/Mg]$ –age slope with an intrinsic scatter of 0.11 dex, while the solar and higher $\log g$ stars produce statistically consistent slopes that are $>1\sigma$ shallower than the lower $\log g$ stars and exhibit intrinsic scatters of 0.078 and 0.17 dex, respectively. For the lower, solar, and higher $\log g$ stars, the corresponding age uncertainties are 3.9, 5.3, and 14 Gyr, and F -test p -value significances are 11.8σ , 7.9σ , and 3.0σ , respectively. The 14 Gyr uncertainty on the higher $\log g$ stars is largely due to a combination of the large intrinsic scatter and the 2σ shallow slope. Summaries of the fit parameters can be found in Table 1.

Ultimately, our $\log g$ results suggest that the most sensitive $[Y/Mg]$ –age relationship occurs for the lower $\log g$ stars,

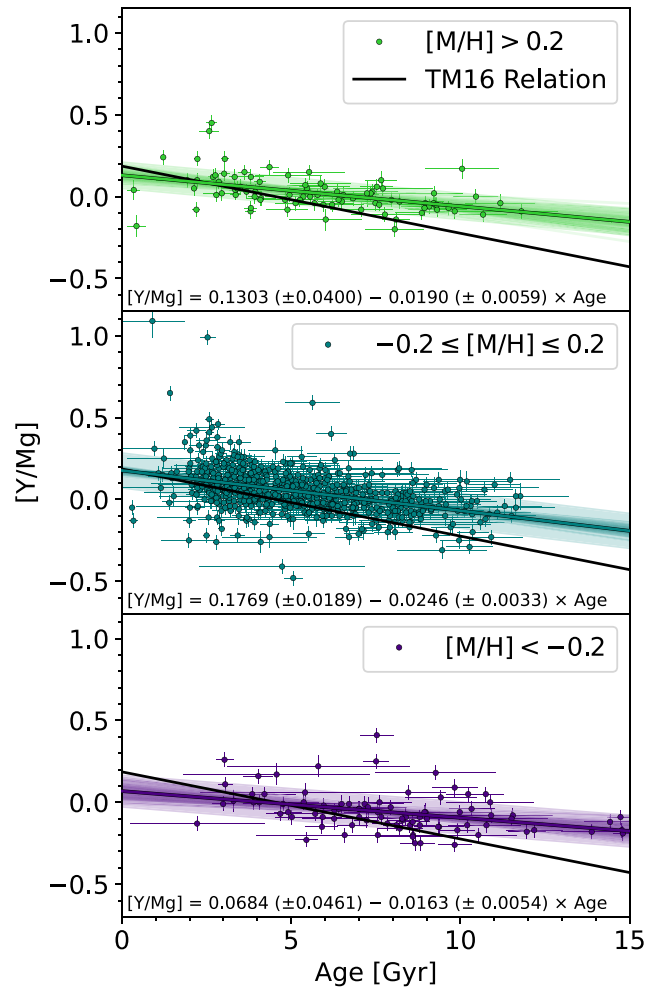


Figure 8. $[Y/Mg]$ vs. stellar age for the reduced **BF18** sample. The top, middle, and bottom panels show metallicities > 0.2 dex, metallicities between -0.2 and 0.2 dex, and metallicities < -0.2 dex, respectively. We plot the best-fitting relations as solid lines and the MCMC realizations as translucent lines underneath. In black we plot the **TM16** best-fit relation.

which are the largest of the three $\log g$ samples. In general, isochrones are most sensitive for these stars and may result in a more precisely measured relationship. We also measure the most uncertain relation for higher $\log g$ stars, which comprise the smallest $\log g$ sample, produce the largest age and intrinsic scatter, and produce the smallest F -test significance.

4.5. The $[Y/Mg]$ Clock and Stellar Metallicity

Feltzing et al. (2017) demonstrated that the $[Y/Mg]$ Clock appears to weaken for subsolar metallicities of ~ -0.5 dex. Therefore, we investigate the reduced **BF18** sample for the presence of a metallicity-dependent slope in the $[Y/Mg]$ Clock. Figure 8 shows the $[Y/Mg]$ –age relationship as a function of metallicity. We do not see any large differences in the age ranges of each metallicity sample. This is unsurprising given the rather flat stellar age–metallicity relation of the Galaxy (Nordström et al. 2004; Haywood et al. 2013; Bergemann et al. 2014).

The top, middle, and bottom panels display the supersolar-, solar-, and subsolar-metallicity stars in the reliable **BF18** sample, respectively. In general, we do not find any significant trends as a function of metallicity. Only the solar-metallicity sample exhibits a $>1\sigma$ difference from the low-metallicity

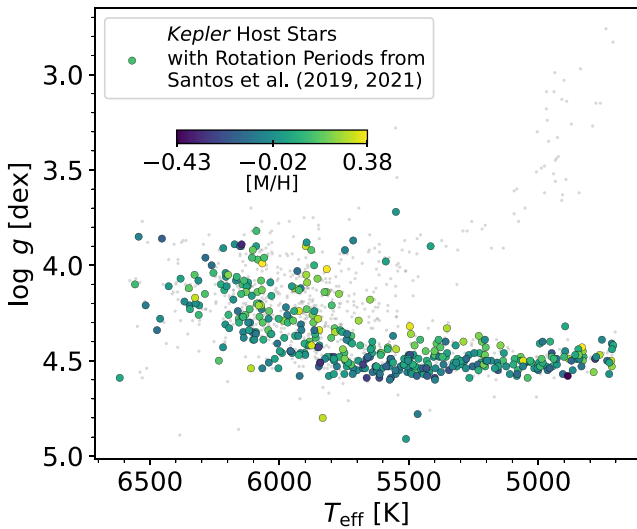


Figure 9. Kiel diagram of Kepler host stars with spectroscopic parameters and $[Y/Mg]$ abundances from BF18. The colored circles represent the 401 stars that have a measured rotation period in Santos et al. (2019) or Santos et al. (2021) and are colored by their metallicity from BF18. Plotted in gray are Kepler host stars without measured rotation periods from Santos et al. (2019) or Santos et al. (2021).

sample. We performed F -tests and found p -value significances all over 3σ , suggesting that each sample is best described by a slope + intercept model over an intercept-only model. Summaries of the fit parameters can be found in Table 1. Because only the low-metallicity sample produces a marginally less sensitive $[Y/Mg]$ –age relationship than the solar-metallicity sample, our results are in general agreement with the Feltzing et al. (2017) conclusion that subsolar-metallicity stars produce weaker $[Y/Mg]$ –age relationships.

5. $[Y/Mg]$ and Stellar Rotation

5.1. Rotation Sample

Isochrone ages are not informative for lower main-sequence stars, as they do not evolve quickly enough. Therefore, we can try to use other, more sensitive age indicators for low-mass stars, such as stellar rotation periods (Barnes 2007; Mamajek & Hillenbrand 2008; Soderblom 2010; van Saders et al. 2016; Curtis et al. 2019), to compare directly against $[Y/Mg]$.

First, we cross-matched the BF18 data with the rotation periods (P_{rot}) provided by Santos et al. (2019) and Santos et al. (2021), which supersedes the McQuillan et al. (2013) and McQuillan et al. (2014) catalogs. We plot this sample in Figure 9. The colored circles, which represent stars with rotation periods, span the full range in T_{eff} , include a few subgiants and no giants, and range in metallicity from -0.43 to 0.38 dex. Unlike luminosity and T_{eff} , rotation periods clearly evolve with time for stars cooler than 5400 K, even if their exact rotation period–age relations remain a subject of debate. Unfortunately, the TM16 sample has only seven stars with light-curve-constrained rotation periods (Lorenzo-Oliveira et al. 2019), so we do not analyze them here and instead focus on the BF18 sample.

We translated the measured rotation periods to rotation ages using *kiauhoku* (Claytor et al. 2020) and the BF18 spectroscopic T_{eff} , $\log g$, and metallicity. We used the fast launch YREC models of van Saders & Pinsonneault (2013) with the

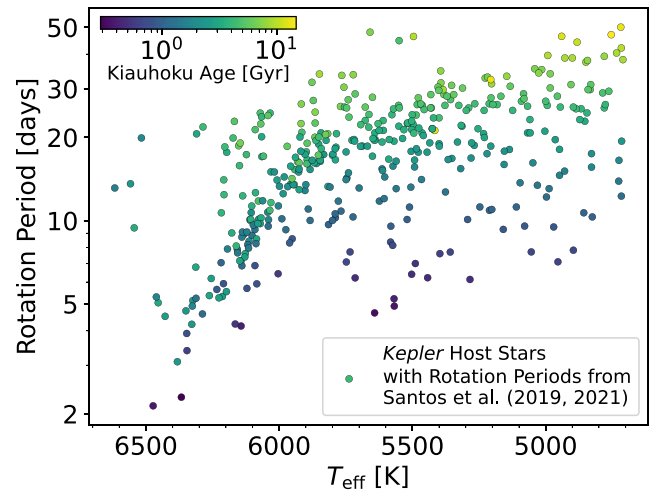


Figure 10. Rotation period vs. effective temperature for the 401-star sample highlighted in Figure 9. Stars are colored by their *kiauhoku* age on a logarithmic scale.

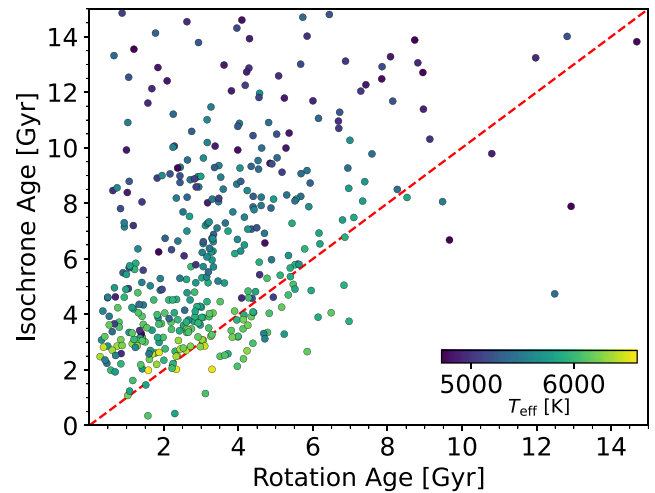


Figure 11. Dartmouth isochrone ages from BF18 vs. rotation ages from *kiauhoku*. Stars are colored by their T_{eff} , and the 1:1 line is represented by the red dashed line.

weakened magnetic braking prescription of van Saders et al. (2016) to produce rotation ages. Figure 10 shows the same sample in $P_{\text{rot}}-T_{\text{eff}}$ space, with the derived ages from *kiauhoku*. We observe a clustering of stars in a band going from 10 days at 6100 K up to 20 days at 5500 K with similar colors, representing ages common for stars in the Kepler field and solar neighborhood. The stars that appear above that cluster are subgiants, as expected. The apparent pileup at long periods was addressed in David et al. (2022) and appears to be the signature of weakened magnetic braking (van Saders et al. 2016); we account for this weakened magnetic braking in the *kiauhoku* modeling.

5.2. Comparing Rotation and Isochrone Ages

In Figure 11 we show a comparison of the BF18 isochrone ages and rotation ages from *kiauhoku*. We find that rotation-based ages are systematically younger than isochrone-based ages. The rotation age histogram peaks at ≈ 2.9 Gyr with only six stars older than 10 Gyr, while the BF18 isochrone age

Table 2
[Y/Mg]–Rotation Age Best-fit Relations

Sample	Slope (m)	σ_m	Intercept (b)	σ_b	Intrinsic Scatter (c)	σ_{Age} (Gyr)	F -test (σ)
16. BF18	−0.0228	0.0044	0.121	0.016	0.11	5.5	8.6
17. BF18 solar analogs	−0.0281	0.0070	0.139	0.024	<0.001	2.8	4.7
18. BF18 solar twins	−0.0317	0.0099	0.162	0.029	<0.001	2.3	4.2
19. BF18 5000 K $\leq T_{\text{eff}} \leq$ 6200 K	−0.0166	0.0042	0.116	0.016	0.096	7.1	6.2
20. BF18 dwarfs \cap 5000 $\leq T_{\text{eff}} \leq$ 6200 K	−0.0222	0.0043	0.118	0.015	0.065	4.6	8.7
21. BF18 dwarfs \cap 5900 K $\leq T_{\text{eff}} \leq$ 6200 K	−0.020	0.010	0.107	0.026	0.042	4.7	2.5
22. BF18 dwarfs \cap 5600 K $\leq T_{\text{eff}} \leq$ 5900 K	−0.0319	0.0071	0.153	0.024	0.039	3.2	5.7
23. BF18 dwarfs \cap 5000 K $\leq T_{\text{eff}} \leq$ 5600 K	−0.0201	0.0064	0.111	0.026	0.081	5.8	5.7
24. BF18 dwarfs \cap 5000 K $\leq T_{\text{eff}} \leq$ 6200 K \cap [M/H] > 0.2	−0.0273	0.0080	0.074	0.031	<0.001	3.8	4.3
25. BF18 dwarfs \cap 5000 K $\leq T_{\text{eff}} \leq$ 6200 K \cap −0.2 \leq [M/H] \leq 0.2	−0.0200	0.0045	0.119	0.016	0.065	5.0	7.4
26. BF18 dwarfs \cap 5000 K $\leq T_{\text{eff}} \leq$ 6200 K \cap [M/H] < −0.2	−0.015	0.046	0.06	0.21	0.086	6.5	0.8

Note. Best-fit relations computed for the various [Y/Mg]–rotation age comparisons detailed in Section 5. All equations are of the form $[Y/Mg] = m \times \text{age}_{\text{rot}} + b$, and 1σ uncertainties are quoted for each parameter. We fit for intrinsic scatter by adding the term $c^2 \cos^2(\arctan(m))$ to the variance in our MCMC analysis and report σ_{age} , which is the corresponding scatter in age in units of Gyr about the best-fit relation. We also include our F -test results in the final column, indicating the corresponding significance of the p -value in units of σ at which the data prefer two-parameter fits (slope plus intercept) over one-parameter fits (intercept only). We plot the summary statistics for this table’s rows 16–26 in columns 16–26 of Figure 13, respectively.

histogram peaks at ≈ 3.5 Gyr with 63 stars older than 10 Gyr. The solar neighborhood age distribution peaks around 3 Gyr and has a few stars older than 10 Gyr (Lin et al. 2018, and references therein), which matches our rotation ages better than the **BF18** isochrone ages. For stars at solar and cooler T_{eff} , rotation is a more sensitive metric of age. Consequently, there is much better agreement for stars hotter than 5800 K, where isochrones are more sensitive to higher-mass stars that evolve more quickly across the H-R diagram. This may be part of the reason for why we find shallower relations above—a cool, apparently old star with higher-than-expected [Y/Mg] may actually be a young star, but isochrone ages are too imprecise to tell the difference.

We caution that period–age relations remain a subject of debate. As the sample of stars with known ages and measured periods has increased, the picture of rotational evolution has become increasingly complex. Van Saders et al. (2016) found that stars past middle age appear to undergo dramatically reduced braking; Curtis et al. (2019) and Curtis et al. (2020) highlighted that stars cooler than 5000 K appear to undergo a period of stalled spin-down at early to intermediate ages. Both phenomena affect the period–age relations. Our models account for the weakened braking in old stars; had we not included it, we would have inferred even younger rotation-based ages. The stalled spin-down, which is most likely the effect of internal angular momentum transport (Denissenkov et al. 2010; Spada & Lanzafame 2020), is not included but should primarily impact stars cooler than the bulk of our sample.

5.3. [Y/Mg]–Rotation Age Results

We performed MCMC analyses and bootstrap simulations as described in Section 4. Table 2 includes our best-fit relations for [Y/Mg] versus rotation ages, from the full 401-star sample described by Figures 9 and 10 to solar twins and analogs. In particular, we choose a sample of stars between 5000 and 6200 K because stars cooler than 5000 K may experience core-envelope decoupling 1 Gyr into their evolution, while those hotter than 6200 K should not experience spin-down while on the main sequence owing to the lack of a convective envelope. We have also selected a sample of dwarfs (defined as stars with *kiauhoku*-derived radii below $1.4 R_{\odot}$) between 5000 and

6200 K to avoid the complications of stellar evolution on rotation periods (van Saders & Pinsonneault 2013).

Figure 12 shows the 22 **BF18** solar twins and 273 **BF18** FGK dwarfs ($R_{\star} < 1.4 R_{\odot}$, $5000 \text{ K} \leq T_{\text{eff}} \leq 6200 \text{ K}$) with rotation ages from *kiauhoku*. For the solar twin and broader samples we compute slopes of $m = -0.0317 \pm 0.0099 \text{ dex Gyr}^{-1}$ and $-0.0222 \pm 0.0043 \text{ dex Gyr}^{-1}$, intrinsic scatters of $c < 0.001 \text{ dex}$ and $c = 0.065 \text{ dex}$, age scatters of 2.3 and 4.6 Gyr, and F -test significances of 4.2σ and 8.7σ , respectively. We include the full results in Sample rows 18 and 20 of Table 2.

We also analyze subsamples of the rotating FGK dwarf sample, splitting the data into bins of T_{eff} and metallicity, similar to our isochrone age analysis above. As a function of T_{eff} , we find that the solar T_{eff} stars produce the most sensitive relation, with small intrinsic scatter ($c = 0.039 \text{ dex}$), age scatter ($\sigma_{\text{Age}} = 3.2 \text{ Gyr}$), and a 5.7σ significant F -test p -value. The high- and low- T_{eff} bins produce statistically consistent slopes, although the high- T_{eff} stars produce a much more uncertain relation that does not prefer the slope + intercept model over the intercept-only model at 3σ significance.

As a function of metallicity, we find statistically similar slopes for the supersolar-, solar-, and subsolar-metallicity bins. In particular, the subsolar-metallicity sample’s slope is $< 1\sigma$ significant, and its F -test favors a slope + intercept fit at only 0.8σ , suggesting that there is no significant trend in [Y/Mg] as a function of age. The supersolar-metallicity sample has the most sensitive relation and the lowest corresponding age uncertainty (3.8 Gyr), but given the lack of a clear trend as a function of metallicity, it is hard to conclude anything confidently.

Overall, we find that the most sensitive and tightest [Y/Mg]–rotation age relations occur for solar twins and analogs. For solar twins, we find a relation that is mostly consistent with the **TM16** isochrone-age-based results and similarly suggests that [Y/Mg] is a reliable age indicator for solar twins. However, as we find above, the [Y/Mg]–Age relationship weakens for nonsolar twin dwarfs and subgiant stars. In addition, we find no metallicity trend, which matches the above isochrone metallicity results.

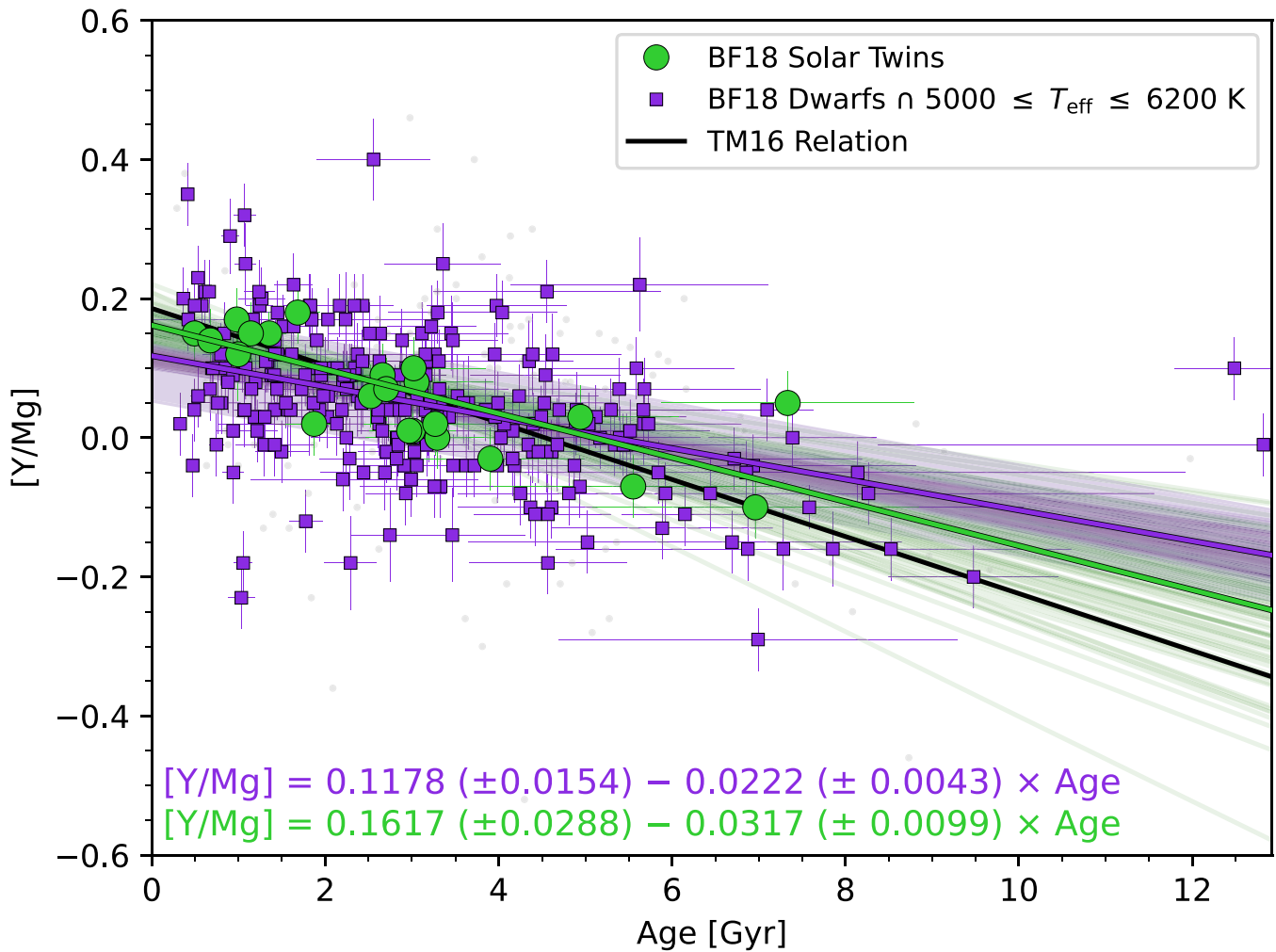


Figure 12. $[Y/Mg]$ vs. rotation age for 22 Kepler host star solar twins (green circles; rotation periods from Santos et al. 2019, 2021, and ages from *kiauhoku*) and 273 Kepler host stars with $5000 \text{ K} \leq T_{\text{eff}} \leq 6200 \text{ K}$ and $R_* < 1.4 R_{\odot}$ (purple squares). We plot the color-matched best-fit relations, in addition to the **TM16** best-fit relation, in black and the full rotation sample as gray circles.

6. Discussion and Conclusion

We confirm that $[Y/Mg]$ works best as a clock for solar twins, but the relationship we find is not as sensitive or as significant as those reported by Nissen (2015), **TM16**, and Spina et al. (2016). We also find that the $[Y/Mg]$ –Age relation weakens for nonsolar-type stars in T_{eff} , $\log g$, and metallicity, in agreement with Feltzing et al. (2017). Unfortunately, the **BF18** sample is composed solely of Kepler host stars, and their location in the solar neighborhood (most within 1 kpc; Brewer et al. 2015) prevents us from directly comparing our results to Anders et al. (2018) and Titarenko et al. (2019) in evaluating Galactic location-dependent $[Y/Mg]$ –age relationships.

In addition, the slope for **BF18** subsolar $\log g$ stars ($m = -0.0309 \pm 0.0037 \text{ dex Gyr}^{-1}$) is statistically consistent with the **BF18** solar twins’ slope ($m = -0.0370 \pm 0.0071 \text{ dex Gyr}^{-1}$), in agreement with Slumstrup et al. (2017), which found a similar $[Y/Mg]$ –age trend for core helium burning giant stars in open clusters to the solar twins in **TM16**. We do note that the **BF18** isochrone fitting was not specifically tuned for giant stars, where different physical ingredients in the models become important when trying to determine an isochrone age (Tayar et al. 2017; Choi et al. 2018; Tayar et al. 2022), preventing a direct comparison to the results of Slumstrup et al.

(2017) and Casamiquela et al. (2021). We also are wary of the isochrone method’s varying sensitivity over the range of T_{eff} and $\log g$ investigated here and its potential to bias our best-fit relations. In general, we show that the $[Y/Mg]$ –Age relation is useful but of varying utility depending on the stellar sample of interest.

We present the first comparison of $[Y/Mg]$ and rotation ages and find that the behavior of $[Y/Mg]$ with rotation age is consistent with isochrone age comparisons, where the $[Y/Mg]$ Clock performs best for solar twins (Nissen 2015; Tucci Maia et al. 2016; Spina et al. 2016; Feltzing et al. 2017). This holds true even though rotation and isochrone ages differ significantly, especially for subsolar-mass stars. Much like with isochrone ages, $[Y/Mg]$ is typically not as sensitive or precise as a rotation age diagnostic for stars that are not solar twins. We also find significant differences between isochrone and rotation age estimates. We suggest that (1) $[Y/Mg]$ –isochrone age relations should be used for subgiants and (2) $[Y/Mg]$ –Rotation Age relations should be used for subsolar-mass dwarfs. For solar-type dwarfs, both rotation and isochrone $[Y/Mg]$ –Age relations appear to perform similarly. Tables 1 and 2 and Figure 13 summarize our best-fit relations.

Finally, we note that binaries are unlikely to have a significant impact on the analysis done in this paper, as Furlan

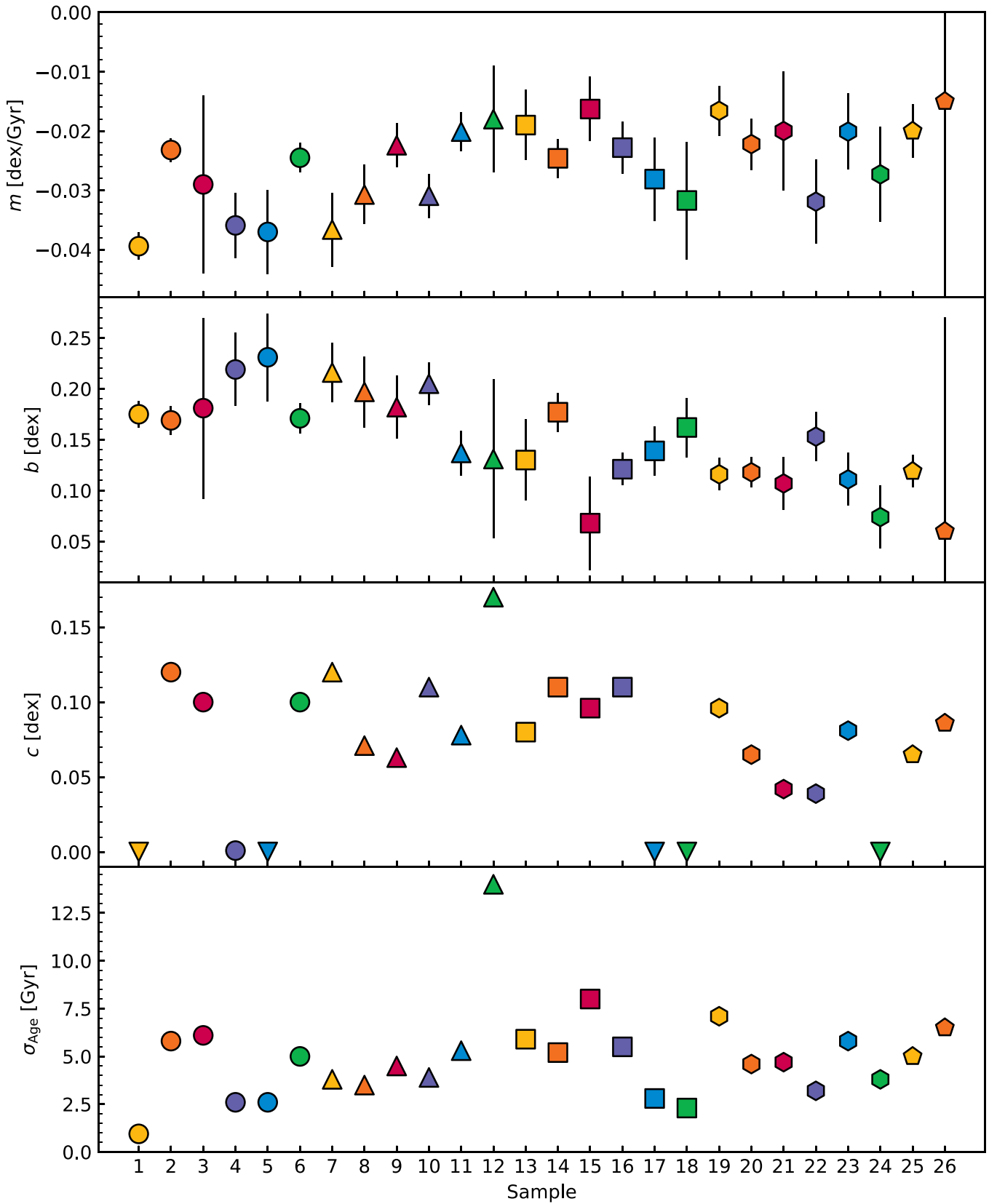


Figure 13. Summary of the best-fit relations detailed in Tables 1 and 2. Samples are numbered according to the numerical value in the Sample column of each table. Panels from top to bottom display the slope (and uncertainty), intercept (and uncertainty), intrinsic scatter, and age uncertainty of each best-fit relation, respectively. In the intrinsic scatter panel, upper limits ($c < 0.001$ dex) are displayed as downward-pointing triangles.

et al. (2017) determined that $\approx 10\%$ of Kepler hosts have adaptive-optics-detected binary companions within $1''$, which is larger than the slit width used in the BF18 spectra ($0.86''$;

Petigura et al. 2017). In addition, only a subset of these stars will affect the BF18 spectroscopic analysis, as (1) double-lined spectroscopic binaries are not included in BF18 (removed by

Petigura et al. 2017) and (2) only systems with moderate mass ratios should produce suspect stellar properties and abundances. Binaries impact the rotation sample even less than the isochrone sample, as Santos et al. (2019, 2021) flag only seven stars as classical pulsator/close-in binary candidates, and the rest do not have a binary flag in either Berger et al. (2018b) or Simonian et al. (2019). For wide binaries, where we do not expect there to be significant impact on stellar parameters or measured abundances, Espinoza-Rojas et al. (2021) show that even coeval, chemically inhomogeneous binaries can display consistent chemical clocks.

We summarize our conclusions as follows:

1. We find that $[Y/Mg]$ -age relations for solar twins and analogs are the most sensitive ($m \lesssim -0.03$ dex Gyr^{-1}) and tightest ($c < 0.001$ dex, $\sigma_{\text{age}} < 2.6$ Gyr) among the FGK stars analyzed in this paper. We find that the BF18 Kepler solar twins produce a $[Y/Mg]$ -age slope that is statistically consistent with the TM16 relation, albeit with an intercept offset that would produce ages different by $\gtrsim 1.5$ Gyr given a measured $[Y/Mg]$. We note that any differences between our relation and those in the literature could be due to nonsolar twin contaminants in our sample or systematics in the abundance or age determinations. We also compared $[Y/Mg]$ to rotation age for the first time and produce similar findings.
2. We do not find any significant trends in the $[Y/Mg]$ Clock as a function of T_{eff} , $\log g$, or metallicity. In general, we find that nonsolar FGK-type samples produce shallower ($m \gtrsim -0.02$ dex Gyr^{-1}) $[Y/Mg]$ -age relations with greater intrinsic scatter ($c > 0.04$ dex) and age scatter ($\sigma_{\text{Age}} > 3.2$ Gyr) than the solar twin and analog samples. However, many of these relations remain statistically significant and may be useful for future related work.
3. We compare isochrone and rotation ages for a subsample of BF18 stars with rotation periods and find significant differences between the isochrone and rotation age estimates. In particular, the rotation ages are systematically younger and match the age of the solar neighborhood better than isochrone ages. We suggest that $[Y/Mg]$ -isochrone age relations should be used for subgiants, $[Y/Mg]$ -rotation age relations should be used for subsolar-mass dwarfs, and both rotation and isochrone ages appear to perform similarly for solar-type dwarfs. Finally, we compared our solar twin $[Y/Mg]$ -isochrone age relation to the literature relations (Table 6 of Delgado Mena et al. 2019) and found a corresponding systematic age uncertainty of ≈ 1.5 Gyr, which we suggest to add in quadrature to any age derived from a $[Y/Mg]$ -age relation.

While the $[Y/Mg]$ Clock is most useful for solar twins, it can still be applied to more diverse FGK stars. It also does not preclude the use of an ensemble of age indicators to more robustly constrain the ages of field stars. We look forward to future investigations leveraging the now-diverse set of age indicators for Kepler and soon TESS planet host stars.

We thank the referee for the useful comments that improved the paper. We also thank Eugene Magnier, Christoph Baranec, Aleezah Ali, Tom Barclay, Vanshree Bhalotia, Casey Brinkman, Ashley Chontos, Marc Hon, Maryum Sayeed, Nicholas Saunders, Aldo Sepulveda, Jamie Tayar, Lauren Weiss, and

Jingwen Zhang for helpful discussions in addition to feedback on the figures. A portion of T.A.B.'s research was supported by an appointment to the NASA Postdoctoral Program at the NASA Goddard Space Flight Center, administered by Universities Space Research Association and Oak Ridge Associated Universities under contract with NASA. T.A.B. and D.H. acknowledge support by a NASA FINESST award (80NSSC19K1424). D.H. also acknowledges support from the Alfred P. Sloan Foundation and NASA grant 80NSSC19K0597. E.G. acknowledges support from NSF award AST-187215.

Software: emcee (Foreman-Mackey et al. 2013), kiau-hoku (Claytor et al. 2020), matplotlib (Hunter 2007), numpy (Harris et al. 2020), pandas (McKinney 2010; Reback et al. 2021), scipy (Virtanen et al. 2020), TOPCAT (Taylor 2005).

ORCID iDs

Travis A. Berger  <https://orcid.org/0000-0002-2580-3614>
 Jennifer L. van Saders  <https://orcid.org/0000-0002-4284-8638>
 Daniel Huber  <https://orcid.org/0000-0001-8832-4488>
 Eric Gaidos  <https://orcid.org/0000-0002-5258-6846>
 Joshua E. Schlieder  <https://orcid.org/0000-0001-5347-7062>
 Zachary R. Clayton  <https://orcid.org/0000-0002-9879-3904>

References

- Anders, F., Chiappini, C., Santiago, B. X., et al. 2018, *A&A*, 619, A125
 Angus, R., Beane, A., Price-Whelan, A. M., et al. 2020, *AJ*, 160, 90
 Angus, R., Morton, T., Aigrain, S., Foreman-Mackey, D., & Rajpaul, V. 2018, *MNRAS*, 474, 2094
 Barnes, S. A. 2007, *ApJ*, 669, 1167
 Bergemann, M., Ruchti, G. R., Serenelli, A., et al. 2014, *A&A*, 565, A89
 Berger, T. A., Howard, A. W., & Boesgaard, A. M. 2018a, *ApJ*, 855, 115
 Berger, T. A., Huber, D., Gaidos, E., & van Saders, J. L. 2018b, *ApJ*, 866, 99
 Berger, T. A., Huber, D., Gaidos, E., van Saders, J. L., & Weiss, L. M. 2020a, *AJ*, 160, 108
 Berger, T. A., Huber, D., van Saders, J. L., et al. 2020b, *AJ*, 159, 280
 Bernstein, R., Shectman, S. A., Gunnels, S. M., Mochnacki, S., & Athey, A. E. 2003, *Proc. SPIE*, 4841, 1694
 Boesgaard, A. M., Lum, M. G., Deliyannis, C. P., et al. 2016, *ApJ*, 830, 49
 Borucki, W. J., Koch, D., Basri, G., et al. 2010, *Sci*, 327, 977
 Brewer, J. M., & Fischer, D. A. 2018, *ApJS*, 237, 38
 Brewer, J. M., Fischer, D. A., Basu, S., Valenti, J. A., & Piskunov, N. 2015, *ApJ*, 805, 126
 Casamiquela, L., Soubiran, C., Jofré, P., et al. 2021, *A&A*, 652, A25
 Choi, J., Dotter, A., Conroy, C., & Ting, Y.-S. 2018, *ApJ*, 860, 131
 Clayton, Z. R., van Saders, J. L., Santos, Á. R. G., et al. 2020, *ApJ*, 888, 43
 Creevey, O. L., Metcalfe, T. S., Schultheis, M., et al. 2017, *A&A*, 601, A67
 Curtis, J. L., Agüeros, M. A., Douglas, S. T., & Meibom, S. 2019, *ApJ*, 879, 49
 Curtis, J. L., Agüeros, M. A., Matt, S. P., et al. 2020, *ApJ*, 904, 140
 da Silva, R., Porto de Mello, G. F., Milone, A. C., et al. 2012, *A&A*, 542, A84
 David, T. J., Angus, R., Curtis, J. L., et al. 2022, *ApJ*, 933, 114
 Deepak, Reddy, B. E. 2019, *MNRAS*, 484, 2000
 Delgado Mena, E., Moya, A., Adibekyan, V., et al. 2019, *A&A*, 624, A78
 Denissenkov, P. A., Pinsonneault, M., Terndrup, D. M., & Newsham, G. 2010, *ApJ*, 716, 1269
 Dotter, A., Chaboyer, B., Jevremović, D., et al. 2008, *ApJS*, 178, 89
 Edvardsson, B., Andersen, J., Gustafsson, B., et al. 1993, *A&A*, 500, 391
 Espinoza-Rojas, F., Chanamé, J., Jofré, P., & Casamiquela, L. 2021, *ApJ*, 920, 94
 Feltzing, S., Howes, L. M., McMillan, P. J., & Stokutė, E. 2017, *MNRAS*, 465, L109
 Fernández, D., Figueras, F., & Torra, J. 2008, *A&A*, 480, 735
 Foreman-Mackey, D., Hogg, D. W., Lang, D., & Goodman, J. 2013, *PASP*, 125, 306
 Fulton, B. J., & Petigura, E. A. 2018, *AJ*, 156, 264
 Furlan, E., Ciardi, D. R., Everett, M. E., et al. 2017, *AJ*, 153, 71
 Gaia Collaboration, Brown, A. G. A., Vallenari, A., et al. 2018, *A&A*, 616, A1
 Gaidos, E., Hirano, T., Mann, A. W., et al. 2020, *MNRAS*, 495, 650

- Harris, C. R., Millman, K. J., van der Walt, S. J., et al. 2020, *Natur*, **585**, 357
- Haywood, M., Di Matteo, P., Lehnert, M. D., Katz, D., & Gómez, A. 2013, *A&A*, **560**, A109
- Hogg, D. W., Bovy, J., & Lang, D. 2010, arXiv:1008.4686
- Holmberg, J., Nordström, B., & Andersen, J. 2009, *A&A*, **501**, 941
- Hunter, J. D. 2007, *CSE*, **9**, 90
- Johnson, J. A. 2019, *Sci*, **363**, 474
- Johnson, J. A., Petigura, E. A., Fulton, B. J., et al. 2017, *AJ*, **154**, 108
- Kjeldsen, H., Bedding, T. R., & Christensen-Dalsgaard, J. 2008, *ApJL*, **683**, L175
- Lin, J., Dotter, A., Ting, Y.-S., & Asplund, M. 2018, *MNRAS*, **477**, 2966
- Lorenz-Oliveira, D., Meléndez, J., Yana Galarza, J., et al. 2019, *MNRAS*, **485**, L68
- Lu, Y. L., Angus, R., Curtis, J. L., David, T. J., & Kiman, R. 2021, *AJ*, **161**, 189
- Magrini, L., Lagarde, N., Charbonnel, C., et al. 2021, *A&A*, **651**, A84
- Makarov, V. V. 2007, *ApJS*, **169**, 105
- Mamajek, E. E., & Hillenbrand, L. A. 2008, *ApJ*, **687**, 1264
- Mazumdar, A. 2005, *A&A*, **441**, 1079
- McKinney, W. 2010, in Proc. 9th Python in Science Conf., ed. S. van der Walt & J. Millman, 56
- McQuillan, A., Mazeh, T., & Aigrain, S. 2013, *ApJL*, **775**, L11
- McQuillan, A., Mazeh, T., & Aigrain, S. 2014, *ApJS*, **211**, 24
- Mentuch, E., Brandeker, A., van Kerkwijk, M. H., Jayawardhana, R., & Hauschildt, P. H. 2008, *ApJ*, **689**, 1127
- Morton, T. D. 2015, isochrones: Stellar model grid package, Astrophysics Source Code Library, ascl:1503.010
- Morton, T. D., Bryson, S. T., Coughlin, J. L., et al. 2016, *ApJ*, **822**, 86
- Nissen, P. E. 2015, *A&A*, **579**, A52
- Nissen, P. E. 2016, *A&A*, **593**, A65
- Nissen, P. E., Silva Aguirre, V., Christensen-Dalsgaard, J., et al. 2017, *A&A*, **608**, A112
- Nordström, B., Mayor, M., Andersen, J., et al. 2004, *A&A*, **418**, 989
- Otí Floranes, H., Christensen-Dalsgaard, J., & Thompson, M. J. 2005, *MNRAS*, **356**, 671
- Petigura, E. A., Howard, A. W., Marcy, G. W., et al. 2017, *AJ*, **154**, 107
- Pinsonneault, M. H., Elsworth, Y. P., Tayar, J., et al. 2018, *ApJS*, **239**, 32
- Piskunov, N., & Valenti, J. A. 2017, *A&A*, **597**, A16
- Ramírez, I., Meléndez, J., Bean, J., et al. 2014, *A&A*, **572**, A48
- Reback, J., McKinney, W., Van den Bossche, J., et al. 2021, pandas-dev/pandas: Pandas 1.3.3 v1.3.3 Zenodo, doi:10.5281/zenodo.5501881
- Santos, A. R. G., Breton, S. N., Mathur, S., & García, R. A. 2021, *ApJS*, **255**, 17
- Santos, A. R. G., García, R. A., Mathur, S., et al. 2019, *ApJS*, **244**, 21
- Sestito, P., & Randich, S. 2005, *A&A*, **442**, 615
- Silva Aguirre, V., Davies, G. R., Basu, S., et al. 2015, *MNRAS*, **452**, 2127
- Simonian, G. V. A., Pinsonneault, M. H., & Terndrup, D. M. 2019, *ApJ*, **871**, 174
- Skrutskie, M. F., Cutri, R. M., Stiening, R., et al. 2006, *AJ*, **131**, 1163
- Skumanich, A. 1972, *ApJ*, **171**, 565
- Slumstrup, D., Grundahl, F., Brogaard, K., et al. 2017, *A&A*, **604**, L8
- Soderblom, D. R. 2010, *ARA&A*, **48**, 581
- Soderblom, D. R., Pilachowski, C. A., Fedele, S. B., & Jones, B. F. 1993, *AJ*, **105**, 2299
- Spada, F., & Lanzafame, A. C. 2020, *A&A*, **636**, A76
- Spina, L., Meléndez, J., Karakas, A. I., et al. 2016, *A&A*, **593**, A125
- Tayar, J., Claytor, Z. R., Huber, D., & van Saders, J. 2022, *ApJ*, **927**, 31
- Tayar, J., Somers, G., Pinsonneault, M. H., et al. 2017, *ApJ*, **840**, 17
- Taylor, M. B. 2005, in ASP Conf. Ser. 347, Astronomical Data Analysis Software and Systems XIV, ed. P. Shopbell, M. Britton, & R. Ebert (San Francisco, CA: ASP), 29
- Titarenko, A., Recio-Blanco, A., de Laverny, P., Hayden, M., & Guiglion, G. 2019, *A&A*, **622**, A59
- Tucci Maia, M., Ramírez, I., Meléndez, J., et al. 2016, *A&A*, **590**, A32
- van Saders, J. L., Ceillier, T., Metcalfe, T. S., et al. 2016, *Natur*, **529**, 181
- van Saders, J. L., & Pinsonneault, M. H. 2013, *ApJ*, **776**, 67
- Vangioni, E., & Olive, K. A. 2019, *MNRAS*, **484**, 3561
- Virtanen, P., Gommers, R., Oliphant, T. E., et al. 2020, *NatMe*, **17**, 261
- Viscasillas Vázquez, C., Magrini, L., Casali, G., et al. 2022, *A&A*, **660**, A135
- Yi, S., Demarque, P., Kim, Y.-C., et al. 2001, *ApJS*, **136**, 417